




Piezoelectric pressure sensors based on GO-modified P(VDF-TrFE) fibers for vacuum applications

Asim Shahzad¹, Zhaofeng Chen^{1,*} , Azhar Ali Haidary², Ahmar Mehmood³, and Zaffar M. Khan⁴

¹International Laboratory of Insulation and Energy Efficiency Materials, College of Material Science and Technology, Nanjing University of Aeronautics and Astronautics (NUAA), Nanjing, People's Republic of China

²Functional Materials and Chemical Sensors Lab (NUAA), College of Material Science and Technology, Nanjing University of Aeronautics and Astronautics (NUAA), Nanjing, People's Republic of China

³Jiangsu Key Laboratory of Electrochemical Energy Storage Technology, College of Material Science and Technology, Nanjing University of Aeronautics and Astronautics (NUAA), Nanjing, People's Republic of China

⁴Department of Aeronautics and Astronautics, Centre for Composite Materials and Smart Structures, Institute of Space Technology, Islamabad, Pakistan

Received: 13 June 2020

Accepted: 2 September 2020

Published online:

19 September 2020

© Springer Science+Business Media, LLC, part of Springer Nature 2020

ABSTRACT

The performance of vacuum insulation panels (VIPs) is greatly determined by their internal vacuum, which is difficult to maintain constant for a long period of time, thus leading to their premature aging. This degradation is mainly caused by the underlying gas and moisture permeation under an extreme environment or from the residual material left inside during the manufacturing process. Hence, the development of smart pressure sensors capable of identifying minute fluctuations in the internal pressure at an initial stage is currently highly desirable in the industry. In the present study, the electrospinning technique was used for the fabrication of poly(vinylidene fluoride-trifluoroethylene) P(VDF-TrFE) and graphene-oxide-modified poly(vinylidene fluoride-trifluoroethylene) GO-P(VDF-TrFE) fiber membranes for piezoelectric pressure-sensing applications. The conventional interdigitated electrode was successfully deposited on the fibrous structure with high continuity in the fingers. The thermal stability and compatibility of the prepared structures were ascertained by performing the thermal characterization. The developed devices revealed high electric output when exposed to the pressure. The GO-P(VDF-TrFE) smart fiber-based device offered admirable response time (0.282 s) and high linearity of $R^2 = 0.99294$, respectively. Our findings will lay a foundation for the establishment of future wireless smart structures capable of detecting small internal pressure (≤ 10 Pa) in many devices such as VIPs and other products even after their installation in building structures.

Address correspondence to E-mail: zhaofeng_chen@163.com

1 Introduction

Structural health monitoring (SHM) has become an essential requirement for the safe operation of complex and costly structures such as aerospace, civil, and mechanical engineering infrastructure, as well as the microelectronics industry [1–13]. Lack of reliable forewarning system can impair the structural integrity, survivability, and operation of engineering structures which may lead to catastrophic results especially in the extreme environments in tropical regions having hot and humid climates. Buildings in these regions with extreme temperatures need enormous workload to maintain the internal atmosphere against a harsh climate, resulting in substantial energy costs as well as losses [14, 15]. To reduce these losses, thermal insulation systems based on inorganic fibrous materials (glass wool and rock wool) and organic foamy materials (expanded polystyrene (EPS), extruded polystyrene (XPS), and phenolic foam) were traditionally employed [16–18]. However, in recent years, a novel thermal insulation technology known as vacuum insulation panels (VIPs) has been introduced successfully in building structures as well as refrigeration industry, pharmaceutical transport boxes, cooling chains, and numerous other applications [19–24]. The life and performance of VIPs are highly dependent on the maintenance of the internal vacuum, which is reported to be challenging to maintain constant for an extended period [25, 26]. Generally, the aging of evacuated panels refers to the variations in the pressure inside or around the system. Various smart structures and materials have been utilized for the detection of such pressure at their initial stage, even in a very minute quantity. The rise of the internal pressure in VIPs is mainly due to the accumulation of moisture and gases in core material or their permeation through envelope film. Consequently, the creation of such internal pressure is the primary aging factor influencing the long-term thermal performance and hence, the service life of a VIP. Although the moisture permeation can easily be measured just by weighing, however, no standard method for the measurement of the internal pressure exists. The most commonly-used method for VIPs internal pressure measurement is a depressurization-based method, which is also known as the foil lift-off method [27]. This whole process is carried out inside a vacuum chamber. However, this technique can only be used on a laboratory scale, and it is more

challenging to monitor the VIP vacuum level in industrial environments after its installation, as well as through its lifespan. Thus, the development of innovative contactless pressure-sensing techniques for monitoring internal pressure is becoming crucial for the VIP industry and other applications which need to maintain a high vacuum.

Self-energy harvesting pressure sensors in the range of subtle pressure (~ 1 Pa–1 kPa) have been studied by various researchers for different applications. Sharma et al. [28] fabricated a 2D pressure sensor by using low-cost, low-temperature standard lithography fabrication technique for the catheter applications. Zang et al. [29] reported 1D nanofibrous structures developed by Persona et al. [30] for the pressure-sensing applications. P(VDF-TrFE)/multi-walled carbon nanotube (MWCNT) composite fibers-based pressure sensor was fabricated by Wang et al. [31] for the healthcare applications. Furthermore, the electrospinning technique has been utilized by several researchers [32–40] for the fabrication of smart fibers for pressure-sensing applications. Our work aims to develop smart fibrous structures for the detection of internal pressure in VIPs, which can also be applicable during their service life. Smart fibers comprising of P(VDF-TrFE) as an electroactive polymer (EAP) and graphene oxide (GO) as nanofillers were prepared for this application. Effect of GO on the microstructure, degree of crystallinity, thermal stability, and dielectric and ferroelectric properties are thoroughly discussed, and the mechanisms responsible for sensing VIPs internal pressure are expounded. We reckon that these smart structures will play an essential role in the structural health monitoring of many pressure-sensitive systems such as VIPs.

2 Experimental section

2.1 Materials

Liquid graphene oxide (GO) was synthesized by a modified hummers method on a laboratory scale. The corresponding typical procedure is already mentioned in detail in our previous publication elsewhere [41]. Poly(vinylidene fluoride-co-trifluoroethylene) P(VDF-TrFE)-70/30 molar ratio was purchased from Piezotech S.A.S, He´singue, France. Acetone and

N,N-dimethylformamide (DMF) were purchased from J&K Scientific Ltd. (Shanghai).

2.2 Methods

A transparent viscous solution for electrospinning was obtained by dissolving 1.5 g of P(VDF-TrFE)_{70:30} in 6 ml of acetone and was magnetically stirred at 350 RPM for 1 h at room temperature. The color of the solution was changed to golden brown when 1 ml of GO was added and stirred for a further 1 h. After the dissolution of GO, 4 ml of DMF was added to the solution, and the stirring speed was increased to 950 RPM for 1 h at 60 °C temperature. The most favorable solution concentration between acetone and DMF was found to be 3:2.

The self-assembled electrospinning unit consists of a syringe pump (LSP01-1B; Ditron-Tech.), the collector drum (locally manufactured), and the high voltage power supply source (HB-Z503-1AC), respectively. The syringe pump contains a plastic syringe with a stainless-steel nozzle (27 G; 210 μm inner diameter). The solution flow rate was set at 5 ml/h, and the collector drum (diameter of 10 cm) to nozzle tip distance was 16 cm, approximately. The rotation speed of the collector drum covered with Al-foil was 1000 RPM. The positive terminal of the high voltage source was connected to the syringe nozzle and the negative one to the grounded cylinder. The applied voltage between 5.47–8.17 kV was found suitable for the fiber preparation. This voltage value was found to be the switching point between the electrospinning and electro spraying process of the solution.

The electrospinning setup, as shown in Fig. 1a, was used for the preparation of aligned fiber membranes of P(VDF-TrFE) and GO-P(VDF-TrFE), as it can be seen in Fig. 1b. The entire process was performed at room temperature and 50%RH humid environment of the laboratory. The prepared array of fibers membrane was given physical support by the Al-foil, and the insulating polyamide film was laminated in between the conductive Al-foil and the active material (fibers).

The sputtering unit (Sykejing VTC-600-2HD) was used for the deposition of copper electrodes over the active layer of fiber material. The target to substrate distance in the sputtering process was 12 cm, and the

stage rotation speed was 6 RPM, respectively. The internal atmosphere was maintained by the flow of Ar gas at the rate of 10 sccm. The prepared sensor device can be seen in Fig. 1c. Cu wires were connected to the deposited Cu-electrodes with the help of conductive silver (Ag) paste. The sensor device was then annealed in a vacuum tube furnace in Ar-atmosphere at 80 °C standing temperature for 8 h.

2.3 Characterizations

Surface morphologies of the powder particles and fiber membranes were studied with a scanning electron microscope (SEM, MIRA3-TESCAN). The phase composition and crystal structure were identified by X-ray diffraction (XRD, Ultima IV, RIGAKU) with Cu K α radiation ($\lambda = 0.15406$ nm) in the 2θ range of 5–80° at a scanning rate of 5° min⁻¹. The thermal analysis of samples was performed by differential scanning calorimetry (DSC) and thermal gravimetric analysis (TGA) (NETZSCH STA 449F5).

2.4 Pressure sensors measurement

Since it was not possible to connect sensors from inside of VIPs to the external signal receiver employing connecting wires, so the pressure-sensing measurements were carried out in a vacuum chamber. The chamber's internal pressure was increased as it rises in VIPs with aging. The sensors were characterized using a self-assembled pressure-sensing setup, as shown in Fig. 2. The setup consisted of a vacuum pump connected to the vacuum chamber to create a vacuum in it. The sensor device connected to the amplifier (BZ2101-1-1) was placed in the chamber. The backside of the sensor device was taped to the device-holding plate. The internal environment of the vacuum chamber was evacuated as that of the vacuum insulation panel (VIP). As the vacuum releases gradually, the pressure exerts on the sensor, which produces electrical signals by rearranging dipoles under piezoelectric phenomenon. Subsequently, the generated signals were then transferred to the amplifier, which amplifies the signals and sends them to the oscilloscope (Rigol DS1062CA) to collect and record the data. Finally, the recorded data are displayed on a computer screen.

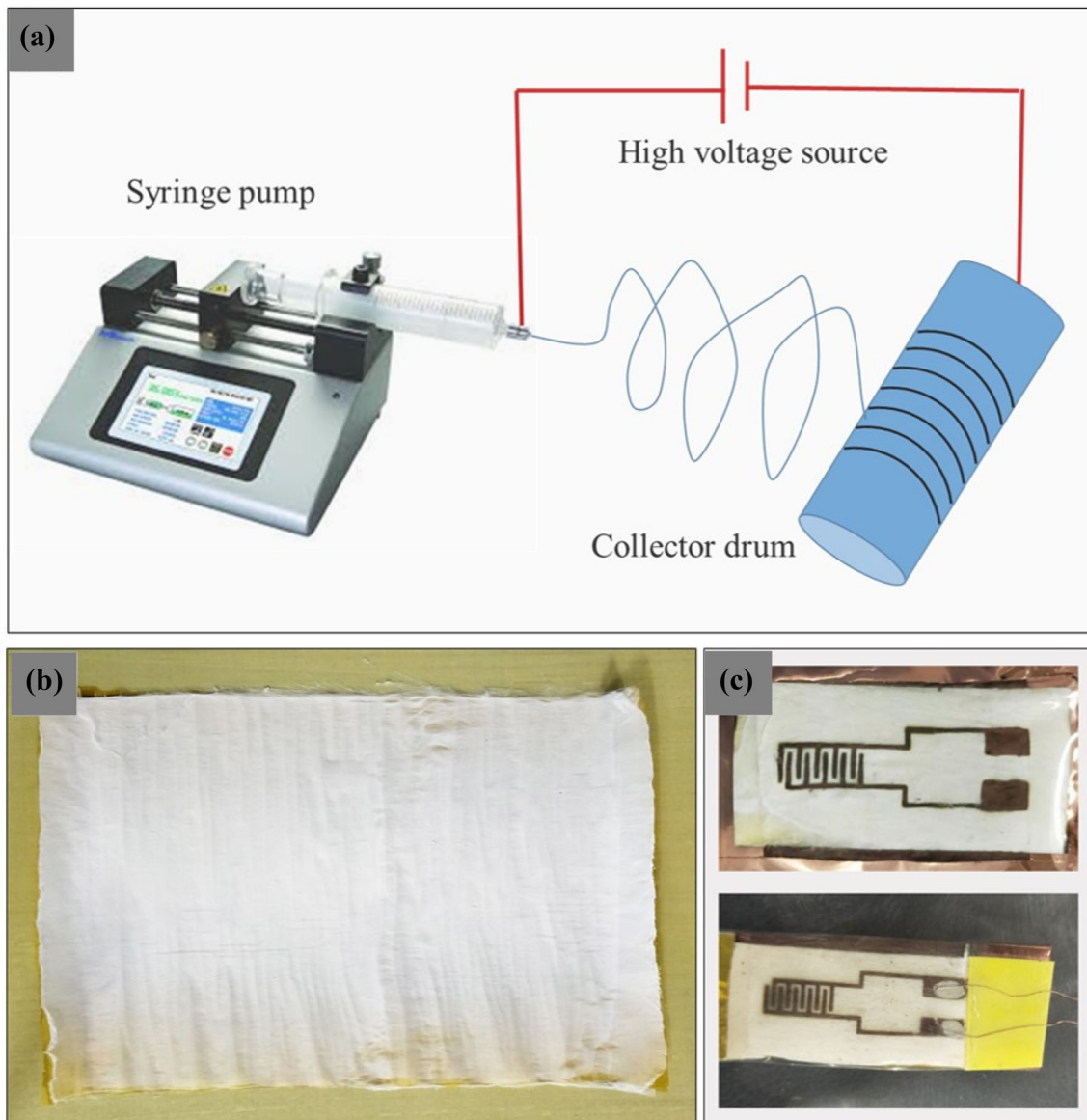


Fig. 1 **a** Schematic diagram for the electrospinning system. **b** Prepared smart fiber membrane laminated over polyamide film. **c** Photographs of the prepared sensor device

3 Results and discussions

3.1 Morphology

The microstructures of the prepared polymeric P(VDF-TrFE) and composite GO-P(VDF-TrFE) smart fibers were analyzed by the scanning electron microscope (SEM). Figure 3a shows the micrographs of the P(VDF-TrFE)_{70:30} nanoparticles having an average diameter of 400 nm. Figure 3b represents a piezoelectric film formed because of the unwanted electrospinning process. Instead of electrospinning, the electrospinning process occurred due to the lower

solution density, improper solution flow rate through the needle, and very high voltage supply. The beads formed, as in Fig. 3c, were due to the imbalance between the solution flow rate and voltage supply concerning the solution density. In this case, the solution flow rate (0.7 ml/h) was very low; however, the applied voltage (18 kV) was very high. Besides this, the needle's larger inner diameter (0.41 mm) was also responsible for the formation of the bead. The higher voltage supply also caused the degree of instability of the jet from the needle's tip to the collector drum, resulting in the wide range distribution

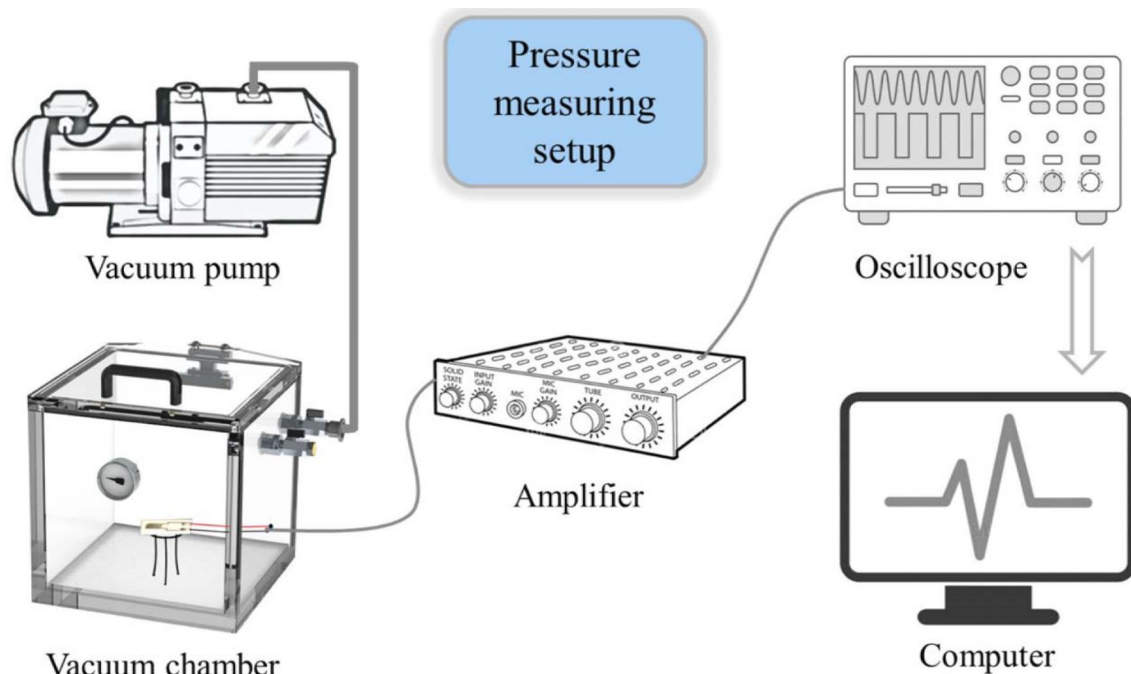


Fig. 2 Schematic illustration of homemade pressure measurement setup with a vacuum chamber similar to the VIPs mechanism

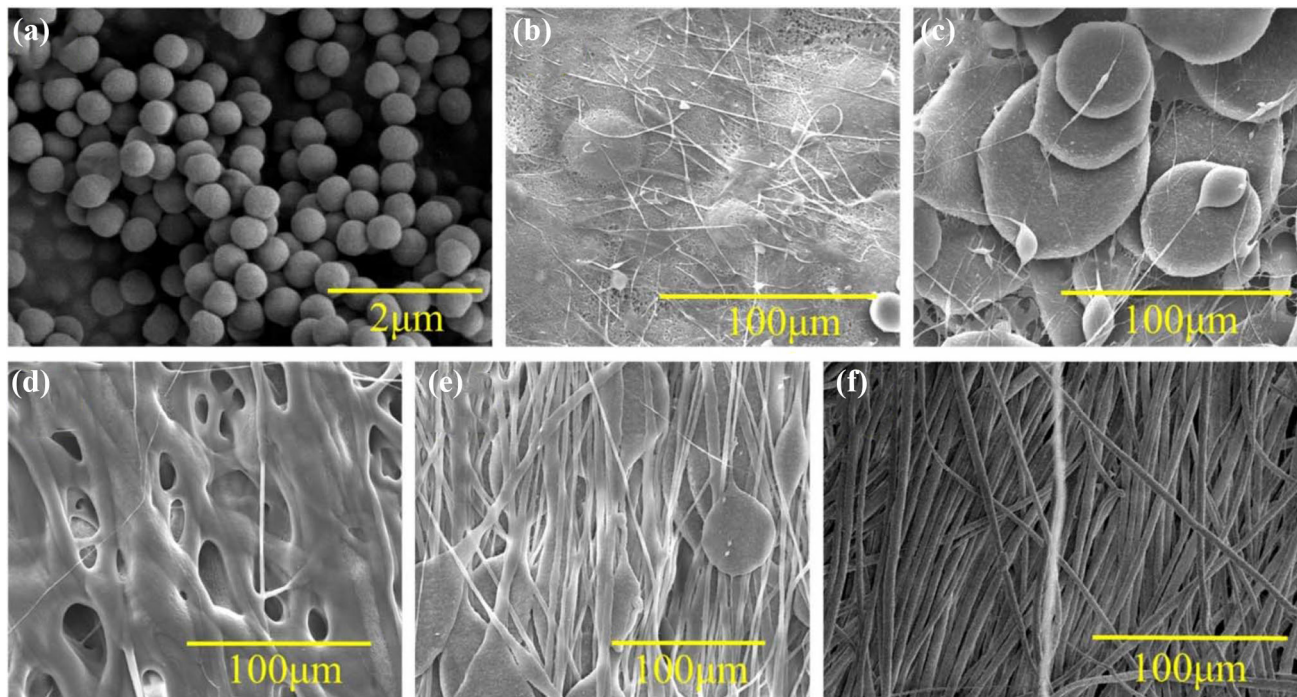


Fig. 3 SEM micrographs of raw material and prepared smart fibers. **a** P(VDF-TrFE)_{70:30} nanoparticles, **b** film formed by electrospinning, **c** droplets formed as a result of electrospinning, **d** deformed fibers, **e** beaded fibers, **f** linearly aligned smart fibers

of solution droplets. The deformed fibers film can be seen in Fig. 3d. The applied voltage, solution density, and the flow rate were optimum; however, the distance between the needle tip and collector drum was

observed to be too short. The solution flight time was not enough to elongate the fibers and evaporate the solvents, due to which the surfaces of the fibers were diffused together. The beaded fibers can be seen in

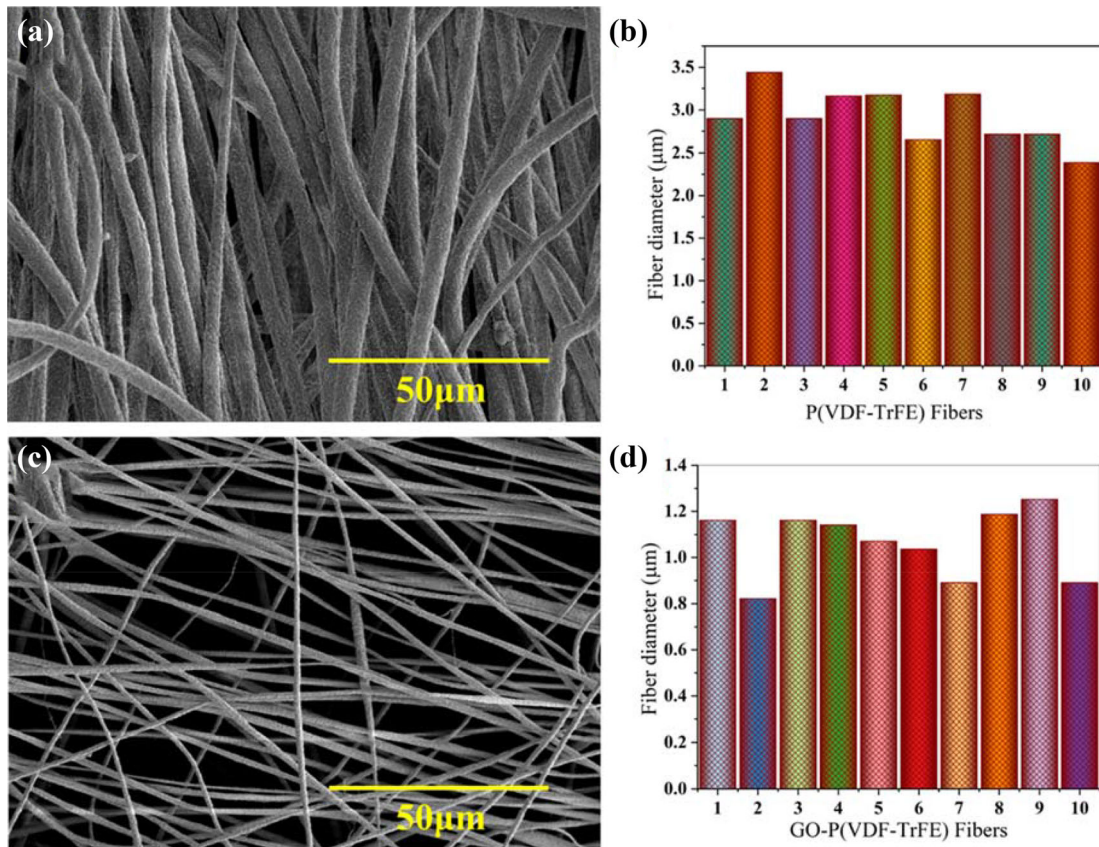


Fig. 4 SEM micrographs and size analysis of P(VDF-TrFE) fibers (a, b), and GO-P(VDF-TrFE) fibers (c, d)

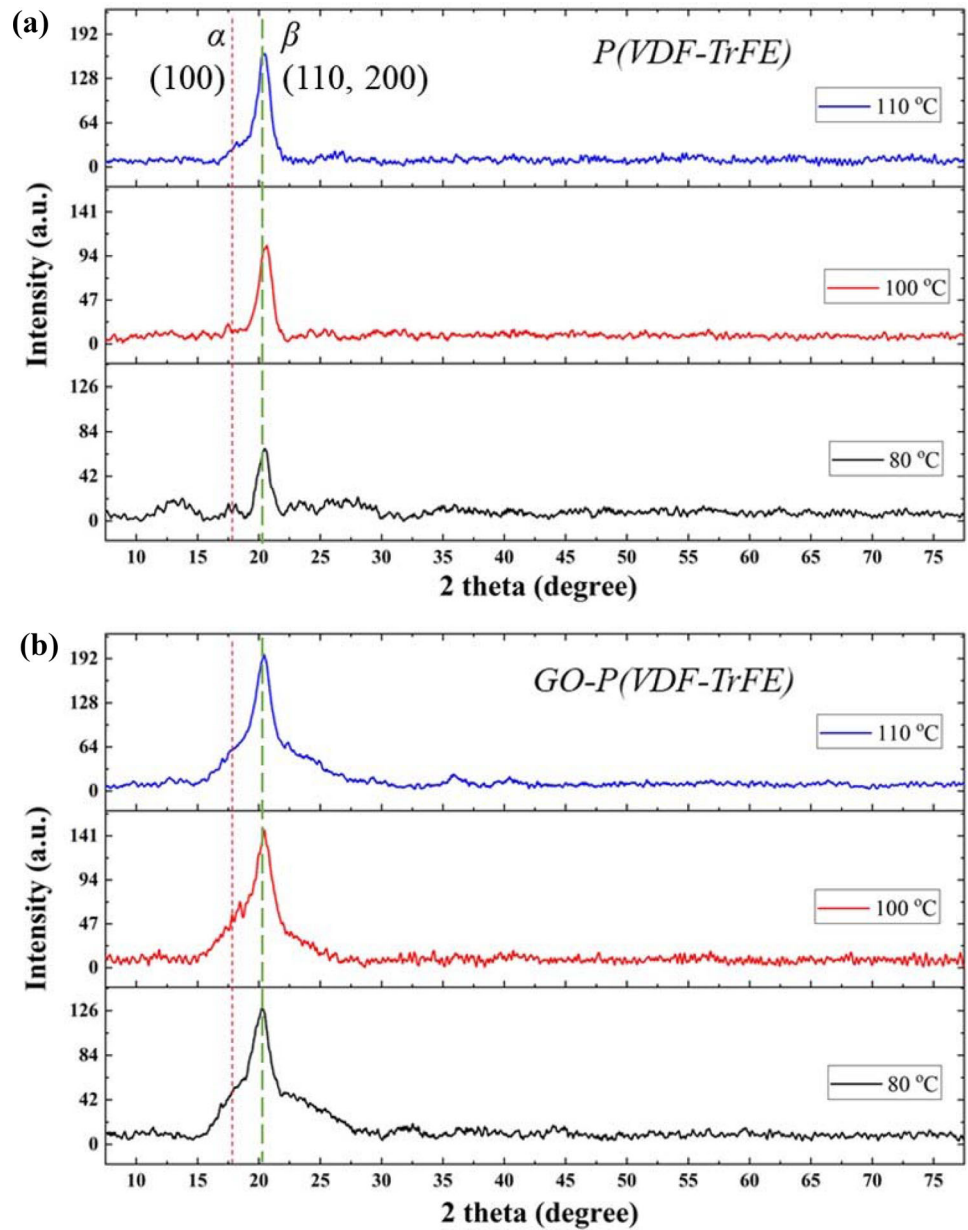
Fig. 3e, where fiber shapes are in the form of stripes, and their diameters are not homogenous. This happened due to the higher concentration of DMF compared to that of acetone in the prepared solution. This issue was fixed by adjusting DMF and acetone ratio at 2:3, which resulted in the formation of a homogeneous and aligned array of fibers, as depicted in Fig. 3f. When the acetone quantity is higher in the solvent, the solution rapidly solidifies due to the high evaporating rate of acetone [42]. Such fibers were formed by adjusting several processing parameters such as a solution flow rate through the needle at 5 ml/h, the syringe needle (27 G sized) having an inner diameter of 210 μm, and the needle to collector distance at 15 cm, respectively. The high voltage supply rate was of utmost importance as it was the main driving force of the electrospinning process. It was found that above 8.17 kV, the electrospinning process changed to the electro spraying process. The highest ratio of fiber formation was achieved when a voltage of 7.47 kV was applied. Similar steps were taken for the preparation of P(VDF-TrFE) polymeric fibers and GO-P(VDF-TrFE) composite fibers.

According to the fiber size analysis from SEM micrographs, as shown in Fig. 4a, c, the variation in fiber diameters of both types of fibers can be observed. The average fiber diameter measured for P(VDF-TrFE) polymeric fibers, as depicted in Fig. 4b, is 2.92 μm, whereas that of GO-P(VDF-TrFE) composite fibers as from Fig. 4d is 1.06 μm, respectively. The diameter of the composite fiber has been reported approximately three times lower because of the evaporation of the additional solvent (ethanol) of the GO solution during the flight time.

3.2 Crystalline structure

The X-ray diffraction (XRD) analysis of smart fibers was carried out to determine the ferroelectric phase formation in the smart fibers. The P(VDF-TrFE) copolymer mainly consists of α , β , and γ -phases, among which higher concentration of the β -phase exhibits the best piezoelectric properties [43, 44]. The piezoelectric behavior of α -phase was transformed to β -phase in the electrospinning process, whereas the β -contents were improved significantly by annealing

Fig. 5 X-ray diffraction patterns of **a** P(VDF-TrFE) fibers membrane, **b** GO-P(VDF-TrFE) fibers membrane at various annealing temperatures



it at various temperatures below the critical temperature. The main electrospinning parameters [45] responsible for this phase transformation are the applied high voltage and the mechanical stretching of a solution (as discussed earlier in Sect. 2.2). The strong electric field due to the applied high voltage (8.17 kV in our work) increases the crystallinity of material by rearranging and aligning the dipoles. The phase transformation from α to β (a peak shift towards $\sim 20^\circ$) occurs during this dipole rearrangement. The mechanical stretching during solution flow from the needle tip to a collector drum permanently aligns the electrical dipoles in the prepared smart

fibers. Furthermore, the intensity of the β -phase was enhanced by annealing the prepared fiber mat at various temperatures, as depicted in Fig. 5a. The annealing process was carried out at 80 °C, 100 °C, and 110 °C, respectively. The prominent peak at $2\theta \approx 19\text{--}20^\circ$ indicates (110) and (200) planes of β -phase of P(VDF-TrFE). Figure 5a, b shows the XRD spectra of both P(VDF-TrFE) polymeric and GO-P(VDF-TrFE) composite fibers. As from Fig. 5a, the peak intensity at $2\theta = 20^\circ$ achieved by annealing P(VDF-TrFE) fibrous membranes at 110 °C indicates the higher β -phase crystallinity of the copolymer. Similarly, the XRD spectra of the composite fibrous membrane in

Fig. 5b also show the improved intensity of β -phase when annealed at 110 °C temperature.

As depicted in Fig. 5b, the peak broadening of composite fibrous membranes, covering area up to $2\theta \approx 23.8^\circ$, indicates the successful doping of graphene oxide (GO) in P(VDF-TrFE) polymeric chains. However, from Fig. 5b, the dramatic increase in the intensity of β -phase was recorded as P(VDF-TrFE) was modified with GO nanofillers. The annealing process at various temperatures further improved the β -phase intensity. Thus, from Fig. 5a, b, the annealing process is proven to be a useful tool to enhance the crystalline region of electrospun nanofibers. By comparing XRD results (Fig. 5a, b) of P(VDF-TrFE) and GO-P(VDF-TrFE), fiber mates annealed at the same temperature prove that the addition of GO nanofiller significantly improves the β -phase contents of the composite.

3.3 Thermal analysis

The differential scanning calorimetry (DSC) results for P(VDF-TrFE) and GO-P(VDF-TrFE) are presented in Fig. 6a; here, T_M refers to the melting temperature during heating which is 159.8 °C for polymeric fibers and 163 °C for composite fibers, respectively. In the heating scan, the melting enthalpy change and the melting point of P(VDF-TrFE) polymer fibers and GO-P(VDF-TrFE) composite fibers were found different. The enthalpy changes of P(VDF-TrFE) was found 20.1 J/g, while that of nanofibers was 22.34 J/g, respectively.

A substantial increase of the melting enthalpy change for GO-P(VDF-TrFE) composite fibers was observed, which corresponds to the increase in crystallinity as indicated by the rise in the intensity of β -phase crystal peak in XRD results as shown in Fig. 5. The reason might also be attributed to the transformation from the α -phase to the β -phase. The stability of the crystalline structure can be observed by the absence of any exothermal peak before the melting point [46].

The thermal gravimetric analysis (TGA) results for both P(VDF-TrFE) and GO-P(VDF-TrFE) are shown in Fig. 6b and have been summarized in Table 1, respectively. Their decomposition temperatures were almost similar for both types of fiber membranes, as

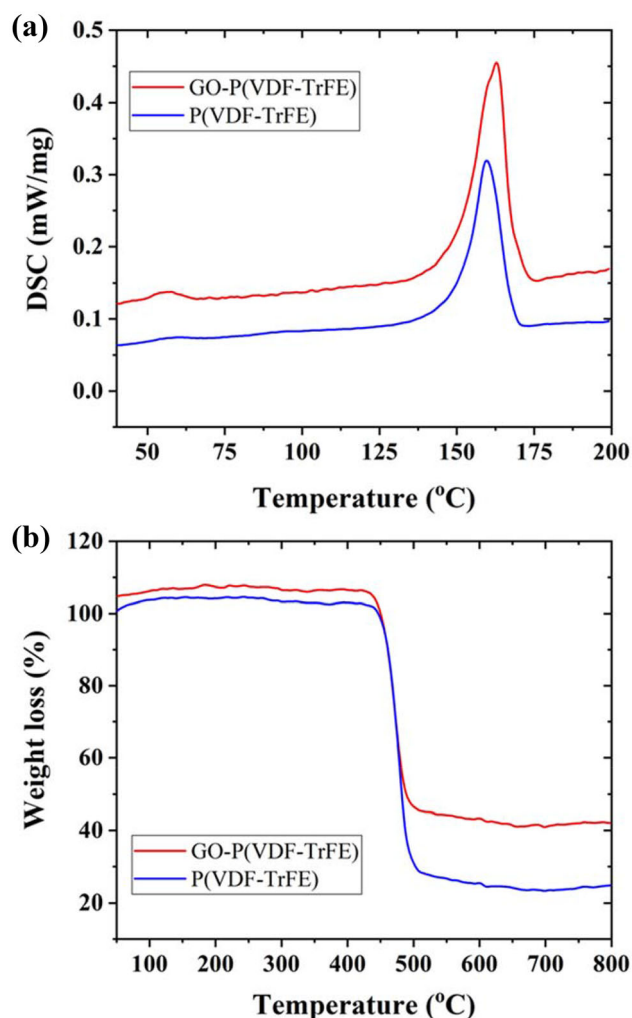


Fig. 6 **a** DSC (heating) traces of P(VDF-TrFE) and GO-P(VDF-TrFE) fibers membrane. **b** TGA traces of P(VDF-TrFE) polymer fibers and GO-P(VDF-TrFE) composite fibers

shown in Table 1. TGA results demonstrated that P(VDF-TrFE) modified with GO had less weight loss as compared to the P(VDF-TrFE) fibers. This lower weight loss was due to the presence of strong bonds between the functional groups of GO such as OH-, COO-, and -C=O with the F₂ and H₂ of P(VDF-TrFE) chains. The inconsistency existed in the weight loss percentage of both types of fibers is possible because of the higher β -phase crystallinity of GO-P(VDF-TrFE) which accords with the XRD results. It also coincided with DSC results, where a slight modification was maintained after melting thereby causing an alteration in TGA traces.

Table 1 Thermal analysis of P(VDF-TrFE) polymer & GO-P(VDF-TrFE) composite fibers

Sample no	Sample name	T_M (°C)	Enthalpy change (J/g)	Decomposition temperature (°C)
1	P(VDF-TrFE)	159.8	20.1	482
2	GO-P(VDF-TrFE)	163.0	22.34	488

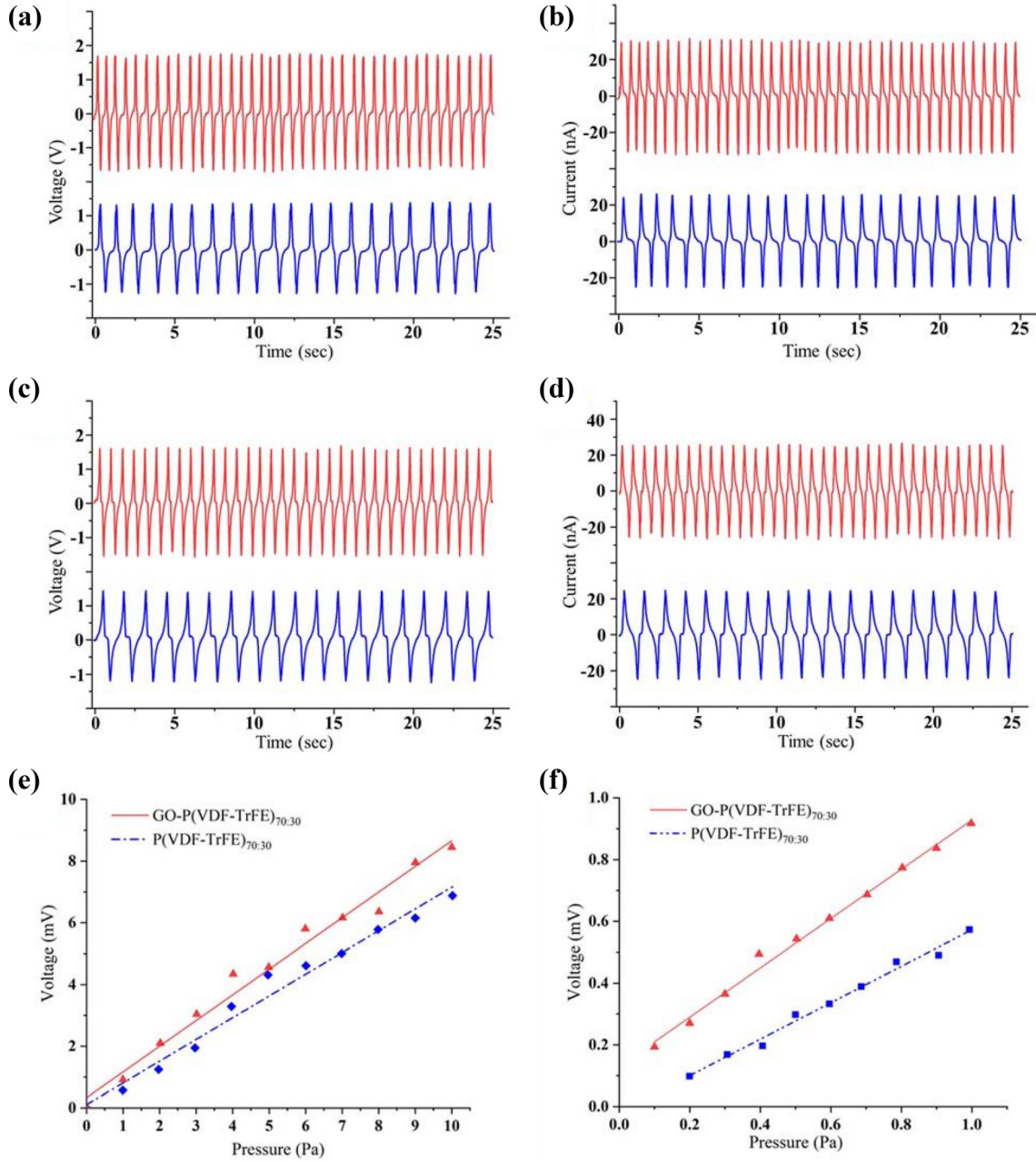


Fig. 7 Electric output of smart fibers membrane devices for exerted frequencies (a–d) of 5 Hz (blue) and 10 Hz (red). The output signals of open-circuit voltage and short-circuit current for

GO-P(VDF-TrFE) (a, b), and P(VDF-TrFE) (c, d)-based devices. Measured short-circuit output current (e, f) Plotted line of a sensor’s measured peak-to-peak voltage (Color figure online)

The maximum operating temperature of VIPs in building applications is reported to be 80 °C [28]. From the above results, the melting temperature (T_M) of smart composite fibers has been found far higher, thus showing high thermal stability under harsh climatic temperatures. As the phase changes in P(VDF-TrFE) occur during electrospinning, the basic chemical structures of α -phase and β -phase remain the same. Therefore, only slight distinctions are observed in the TGA traces.

3.4 Sensor's performance

To determine the reliability of the sensor for detection of VIP's internal pressure, the electric output of P(VDF-TrFE) and GO-P(VDF-TrFE) piezoelectric membrane devices was characterized using home-made equipment. Figure 7 shows pulsed electrical signals composed of positive and negative output peaks, describing the application and releasing of a pressure load as responses to the applied loading. The short-circuit current (Fig. 7b, d) and open voltage (Fig. 7a, c) outputs were in the ranges of 25–30 nA and 1.2–1.7 V, respectively. A slight increase in the output signal of voltage and current has been observed as the frequency rises from 5 to 10 Hz. An increase in the response time (0.282 s) has been noticed with the increasing frequency. It was also found that the signals of both types of sensors remain in a continuous relationship with the applied frequency up to 10 Hz. However, the maximum current and voltage observed for GO-P(VDF-TrFE) sensor were 30 nA and 1.7 V, respectively, as depicted in Fig. 7c, d.

To identify the varying magnitudes of pressure inside the chamber (to emulate the VIPs internal environment), the peak-to-peak voltage from the sensor devices was obtained and plotted, as shown in Fig. 7e, f. The graph depicts a high linear response having adjusted R -squared (R^2) values of 0.98674 for P(VDF-TrFE) device and 0.99294 for GO-P(VDF-TrFE) device, respectively. Furthermore, a higher slope (0.79891 ± 0.02245) is noticed for GO-P(VDF-TrFE) device compared to (0.59066 ± 0.02419) of P(VDF-TrFE) device, indicating a higher sensitivity of smart composite fibers. Here, it can also be stated that the sensor device (GO-P(VDF-TrFE)) having lower fiber diameter shows higher sensitivity as compared to the sensor device (P(VDF-TrFE)). As from Fig. 7f, almost higher signal output has been reported for the

GO-P(VDF-TrFE) device compared to the P(VDF-TrFE) device, revealing higher piezoelectricity of the composite fiber membrane. This is because of the higher surface tension involved in the fiber formation during the electrospinning process, resulting in higher crystallinity in thinner fibers, also proven by the XRD diffractograms. The electrical conductivity of GO is in the range of 1–4 K Ω [41] which results in enhancing the overall electrical properties of the P(VDF-TrFE) smart nanofibers. Here, GO plays a crucial role as a slightly conducting nanofiller and helps to increase the overall electrical properties of the nanocomposite. The large surface area of GO allows more dipole formation and thus improve the charge generation and storage capability of the composite material. This nanofiller supports the nucleation of the piezoelectric polar β -phase of P(VDF-TrFE), also proven by XRD results presented in Fig. 5b. Thus, poled GO-P(VDF-TrFE) nanocomposite fiber mat yielded high piezoelectric-response under the repetitive external pressure. This phenomenon is related to the presence of electrostatic interactions between the C-F dipoles in P(VDF-TrFE) and the OH-, COO-, and -C=O groups in GO. A large number of electrons from the negative functional groups of GO sheets move toward the junction and may transfer into the energy levels of dielectric P(VDF-TrFE). The interactions between the hydrogen and fluorine groups of P(VDF-TrFE) and oxygen functional groups of carbonyl as well as carboxyl groups situated at the basal planes of GO, as shown in Fig. 8 [47], support polymer chain rotation for the formation of electroactive β -phase. Under this situation, an uncompensated charge exists at the interface of GO and PVDF-TrFE, which is the result of the aligned dipoles in the PVDF-TrFE and functional groups in GO. These results suggest their promising applications in health monitoring of vacuum systems, especially for the detection of internal pressure even in the range lower than 10 Pa.

4 Conclusion

Internal pressure is the major factor that affects the service life and performance of the evacuated products in the high-cost applications. Due to the alarming risks, professionals are implementing new strategies for the detection of internal pressure in high-vacuum systems. A highly sensitive β -phase

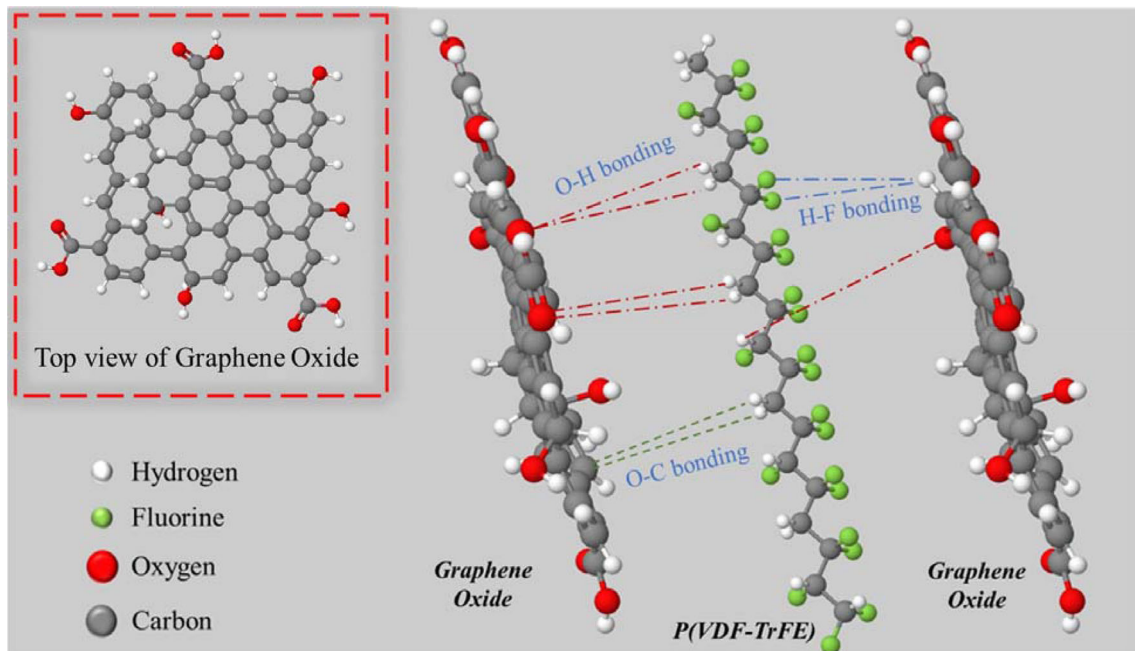


Fig. 8 Schematic diagram demonstrating possible bonding between GO and P(VDF-TrFE) in prepared smart composite fibers

piezoelectric device comprising of P(VDF-TrFE) polymeric and GO-P(VDF-TrFE) composite fiber membranes has been developed by using the electrospinning technique for a tiny pressure detection. Various parameters of electrospinning technique and fiber preparation, especially the switching point between electrospinning and electrospraying process, have been identified. Furthermore, thermal analysis of the prepared smart structures supports their application in VIPs and can easily sustain the working environment of VIPs ($\sim 80^\circ\text{C}$). A quick response time of (0.282 s) has been reported for the prepared composite fiber-based sensor device. The device has a capability to generate signals even at the pressure ≤ 10 Pa, with high linearity (~ 0.99294). In addition, it can be an efficient sensor device as its output response reveals a linear relationship with the applied pressure. Consequently, the prepared devices are considered attractive applicants for their implementation in numerous high-vacuum products for detecting the internal pressure.

Acknowledgements

This work was carried out under a joint project between Nanjing University of Aeronautics and Astronautics (NUAA), China, and the University of

Victoria (UoV), Canada. The project (Grant No. SBZ2019000139) was titled as “Joint Research of Nano modified Ultra-fine Glass Fiber Core with Indulgent Pressure.”

Compliance with ethical standards

Conflict of interest The authors declare that they have no known conflicts of interests that could appear to influence the work reported in this paper.

References

1. X. Qing, W. Li, Y. Wang, H. Sun, Piezoelectric transducer-based structural health monitoring for aircraft applications. *Sensors* **19**(3), 545 (2019). <https://doi.org/10.3390/s19030545>
2. V. Giurgiutiu, Structural health monitoring (SHM) of aerospace composites, *Polymer Composites in the Aerospace Industry* (Elsevier, Amsterdam, 2020), pp. 491–558. <https://doi.org/10.1016/B978-0-08-102679-3.00017-4>
3. E.D. Gregory, W.C. Schneck III, C.A. Leckey, P. Swindell, Simulation assisted guided wave structural health monitoring of aerospace structures, in *AIP Conference Proceedings*, 2019, vol. 2102, no. 1, pp. 130006: AIP Publishing LLC. (2019). <https://doi.org/10.1063/1.5099856>
4. V. Rahul, S. Alokita, K. Jayakrishna, V.R. Kar, M. Rajesh, S. Thirumalini, M. Manikandan, Structural health monitoring of aerospace composites, *Structural Health Monitoring of*

- Biocomposites Fibre-Reinforced Composites and Hybrid Composites* (Woodhead Publishing, Cambridge, 2019), pp. 33–52. <https://doi.org/10.1016/B978-0-08-102291-7.00003-4>
5. Y. Wang, L. Qiu, Y. Luo, R. Ding, "A stretchable and large-scale guided wave sensor network for aircraft smart skin of structural health monitoring, *Structural Health Monitoring* (Sage Publications, London, 2019), pp. 1–16. <https://doi.org/10.1177/1475921719850641>
 6. W.S. Na, J. Baek, A review of the piezoelectric electromechanical impedance based structural health monitoring technique for engineering structures. *Sensors* **18**(5), 1307 (2018). <https://doi.org/10.3390/s18051307>
 7. G. Heo, B. Son, C. Kim, S. Jeon, J. Jeon, Development of a wireless unified-maintenance system for the structural health monitoring of civil structures. *Sensors* **18**(5), 1485 (2018). <https://doi.org/10.3390/s18051485>
 8. C.R. Farrar, K. Worden, An introduction to structural health monitoring. *Philos. Trans. R. Soc. A* **365**(1851), 303–315 (2007). <https://doi.org/10.1098/rsta.2006.1928>
 9. J.P. Lynch, An overview of wireless structural health monitoring for civil structures. *Philos. Trans. R. Soc. A* **365**(1851), 345–372 (2007). <https://doi.org/10.1098/rsta.2006.1932>
 10. B. Chapuis, Introduction to structural health monitoring, *Sensors Algorithms and Applications for Structural Health Monitoring* (Springer, Cham, 2018), pp. 1–11. https://doi.org/10.1007/978-3-319-69233-3_1
 11. H.-P. Chen, *Structural Health Monitoring of Large Civil Engineering Structures* (Wiley, Hoboken, 2018)
 12. H.-R. Shih, W.L. Walters, W. Zheng, J. Everett, Course modules on structural health monitoring with smart materials. *J. Technol. Stud.* **35**(2), 65–73 (2009). <https://doi.org/10.21061/jots.v35i2.a.7>
 13. D. Balageas, C.-P. Fritzen, A. Güemes, *Structural Health Monitoring* (Wiley, Hoboken, 2010)
 14. H.U. Rehman, Experimental performance evaluation of solid concrete and dry insulation materials for passive buildings in hot and humid climatic conditions. *Appl. Energy* **185**, 1585–1594 (2017). <https://doi.org/10.1016/j.apenergy.2016.01.026>
 15. P.M. Congedo, C. Baglivo, G. Centonze, Walls comparative evaluation for the thermal performance improvement of low-rise residential buildings in warm Mediterranean climate. *J. Build. Eng.* **28**, 101059 (2020). <https://doi.org/10.1016/j.jobe.2019.101059>
 16. B.P. Jelle, Traditional, state-of-the-art and future thermal building insulation materials and solutions—properties, requirements and possibilities. *Energy Build.* **43**(10), 2549–2563 (2011). <https://doi.org/10.1016/j.enbuild.2011.05.015>
 17. E. Cuce, P.M. Cuce, C.J. Wood, S.B. Riffat, Toward aerogel based thermal superinsulation in buildings: a comprehensive review. *Renew. Sustain. Energy Rev.* **34**, 273–299 (2014). <https://doi.org/10.1016/j.rser.2014.03.017>
 18. W. Villasmil, L.J. Fischer, J. Worlitschek, A review and evaluation of thermal insulation materials and methods for thermal energy storage systems. *Renew. Sustain. Energy Rev.* **103**, 71–84 (2019). <https://doi.org/10.1016/j.rser.2018.12.040>
 19. M. Alam, H. Singh, M.C. Limbachiya, Vacuum Insulation Panels (VIPs) for building construction industry—a review of the contemporary developments and future directions. *Appl. Energy* **88**(11), 3592–3602 (2011). <https://doi.org/10.1016/j.apenergy.2011.04.040>
 20. Z. Chen, Z.F. Chen, J.L. Qiu, T.Z. Xu, J.M. Zhou, Vacuum insulation panel for green building. *Appl. Mech. Mater.* **71**, 607–611 (2011). <https://doi.org/10.4028/www.scientific.net/AMM.71-78.607>
 21. C. Peng, J. Yang, Structure, mechanism, and application of vacuum insulation panels in Chinese buildings. *Adv. Mater. Sci. Eng.* **2016**, 1–16 (2016). <https://doi.org/10.1155/2016/1358072>
 22. L. Aditya, T.M.I. Mahlia, B. Rismanchi, H.M. Ng, M.H. Hasan, H.S.C. Metselaar, O. Muraza, H.B. Aditya, A review on insulation materials for energy conservation in buildings. *Renew. Sustain. Energy Rev.* **73**, 1352–1365 (2017). <https://doi.org/10.1016/j.rser.2017.02.034>
 23. M. Alam, H. Singh, S. Suresh, D. Redpath, Energy and economic analysis of Vacuum Insulation Panels (VIPs) used in non-domestic buildings. *Appl. Energy* **188**, 1–8 (2017). <https://doi.org/10.1016/j.apenergy.2016.11.115>
 24. S. Verma, H. Singh, Vacuum insulation panels for refrigerators. *Int. J. Refrig.* **112**, 215–228 (2020). <https://doi.org/10.1016/j.ijrefrig.2019.12.007>
 25. E. Wegger, B.P. Jelle, E. Sveipe, Aging effects on thermal properties and service life of vacuum insulation panels. *J. Build. Phys.* **35**(2), 128–167 (2011). <https://doi.org/10.1177/1744259111398635>
 26. X. Di, Y. Gao, C. Bao, S. Ma, Thermal insulation property and service life of vacuum insulation panels with glass fiber chopped strand as core materials. *Energy Build.* **73**, 176–183 (2014). <https://doi.org/10.1016/j.enbuild.2014.01.010>
 27. H. Simmler, S. Brunner, U. Heinemann, H. Schwab, K. Kumaran, P. Mukhopadhyaya, D. Quenard, H. Sallee, K. Noller, E. Kuecukpinar-Niarchos, C. Stramm, M. Tenpierik, H. Cauberg, H. M. Erb, "IEA/ECBCS Annex 39: Vacuum Insulation Panels—Study on VIP-components and Panels for Service Life Prediction of VIP in Building Applications (Subtask A)", Switzerland, (2005), <https://www.osti.gov/etdweb/biblio/21131463>. Accessed 23 Aug 2020

28. T. Sharma, S.-S. Je, B. Gill, J.X. Zhang, Patterning piezoelectric thin film PVDF–TrFE based pressure sensor for catheter application. *Sens. Actuators A* **177**, 87–92 (2012). <https://doi.org/10.1016/j.sna.2011.08.019>
29. Y. Zang, F. Zhang, C.-A. Di, D. Zhu, Advances of flexible pressure sensors toward artificial intelligence and health care applications. *Mater. Horiz.* **2**(2), 140–156 (2015). <https://doi.org/10.1039/C4MH00147H>
30. L. Persano, C. Dagdeviren, C. Maruccio, L. De Lorenzis, D. Pisignano, Cooperativity in the enhanced piezoelectric response of polymer nanowires. *Adv. Mater.* **26**(45), 7574–7580 (2014). <https://doi.org/10.1002/adma.201403169>
31. A. Wang, M. Hu, L. Zhou, X. Qiang, Self-powered wearable pressure sensors with enhanced piezoelectric properties of aligned P(VDF-TrFE)/MWCNT composites for monitoring human physiological and muscle motion signs. *Nanomaterials* **8**(12), 1021 (2018). <https://doi.org/10.3390/nano8121021>
32. Y. Jiang, L. Gong, X. Hu, Y. Zhao, H. Chen, L. Feng, D. Zhang, Aligned P (VDF-TrFE) nanofibers for enhanced piezoelectric directional strain sensing. *Polymers* **10**(4), 364 (2018). <https://doi.org/10.3390/polym10040364>
33. B. Li, F. Zhang, S. Guan, J. Zheng, C. Xu, Wearable piezoelectric device assembled by one-step continuous electrospinning. *J. Mater. Chem. C* **4**(29), 6988–6995 (2016). <https://doi.org/10.1039/x0xx00000x>
34. S. Thenmozhi, N. Dharmaraj, K. Kadirvelu, H.Y. Kim, Electrospun nanofibers: new generation materials for advanced applications. *Mater. Sci. Eng., B* **217**, 36–48 (2017). <https://doi.org/10.1016/j.mseb.2017.01.001>
35. J.K.Y. Lee, N. Chen, S. Peng, L. Li, L. Tian, N. Thakor, S. Ramakrishna, Polymer-based composites by electrospinning: preparation & functionalization with nanocarbons. *Prog. Polym. Sci.* **86**, 40–84 (2018). <https://doi.org/10.1016/j.progpolymsci.2018.07.002>
36. N.M. Aboamera, A. Mohamed, A. Salama, T. Osman, A. Khattab, Characterization and mechanical properties of electrospun cellulose acetate/graphene oxide composite nanofibers. *Mech. Adv. Mater. Struct.* **26**(9), 765–769 (2019). <https://doi.org/10.1080/15376494.2017.1410914>
37. J. Zhao, Y. Yang, W. Yu, Q. Ma, X. Dong, X. Wang, J. Wang, G. Liu, Bi₂MoO₆/RGO composite nanofibers: facile electrospinning fabrication, structure, and significantly improved photocatalytic water splitting activity. *J. Mater. Sci.: Mater. Electron.* **28**(1), 543–552 (2017). <https://doi.org/10.1007/s10854-016-5557-3>
38. C. Brundha, R. Govindaraj, N. Santhosh, M. Senthil Pandian, P. Ramasamy, S. Karuppuchamy, Preparation of one dimensional titanium dioxide nanowires using electrospinning process for dye-sensitized solar cells. *J. Mater. Sci.: Mater. Electron.* **28**(15), 11509–11514 (2017). <https://doi.org/10.1007/s10854-017-6947-x>
39. H. Yu, Y. Li, X. Lan, Z. Liang, Electrospinning preparation and luminescence properties of La₂O₃: Ce³⁺/Tb³⁺ nanofibers. *J. Mater. Sci.: Mater. Electron.* **28**(12), 8832–8836 (2017). <https://doi.org/10.1007/s10854-017-6611-5>
40. N. Chamankar, R. Khajavi, A.A. Yousefi, A.S. Rashidi, F. Golestanifard, Comparing the piezo, pyro and dielectric properties of PZT particles synthesized by sol–gel and electrospinning methods. *J. Mater. Sci.: Mater. Electron.* **30**(9), 8721–8735 (2019). <https://doi.org/10.1007/s10854-019-01197-0>
41. Q. Fatima, A.A. Haidry, Z. Yao, Y. He, Z. Li, L. Sun, L. Xie, The critical role of hydroxyl groups in water vapor sensing of graphene oxide. *Nanoscale Adv.* **1**(4), 1319–1330 (2019). <https://doi.org/10.1039/c8na00135a>
42. Y.J. Hwang, S. Choi, H.S. Kim, Structural deformation of PVDF nanoweb due to electrospinning behavior affected by solvent ratio. *e-Polymers* **18**(4), 339–345 (2018). <https://doi.org/10.1515/epoly-2018-0037>
43. D. Mao, B.E. Gnade, M.A. Quevedo-Lopez, Ferroelectric properties and polarization switching kinetic of poly (vinylidene fluoride-trifluoroethylene) copolymer, *Ferroelectrics-Physical Effects* (InTech, Rijeka, 2011), pp. 78–100
44. N. Weber, Y.-S. Lee, S. Shanmugasundaram, M. Jaffe, T.L. Arinzeh, Characterization and in vitro cytocompatibility of piezoelectric electrospun scaffolds. *Acta Biomater.* **6**(9), 3550–3556 (2010). <https://doi.org/10.1016/j.actbio.2010.03.035>
45. C. Ribeiro, V. Sencadas, J.L.G. Ribelles, S. Lanceros-Méndez, Influence of processing conditions on polymorphism and nanofiber morphology of electroactive poly (vinylidene fluoride) electrospun membranes. *Soft Mater.* **8**(3), 274–287 (2010). <https://doi.org/10.1080/1539445X.2010.495630>
46. X. Ren, *Nanomanufacturing and Analysis of Novel Continuous Ferroelectric PVDF and P (VDF-TrFE) Nanofibers* (The University of Nebraska-Lincoln, Lincoln, 2007)
47. R. Bhunia, S. Gupta, B. Fatma, Prateek, R.K. Gupta, A. Garg, Milli-Watt power harvesting from dual triboelectric and piezoelectric effects of multifunctional green and robust reduced graphene oxide/P (VDF-TrFE) composite flexible films. *ACS Appl. Mater. Interfaces* **11**(41), 38177–38189 (2019). <https://doi.org/10.1021/acsami.9b13360>

Publisher's Note Springer Nature remains neutral with regard to jurisdictional claims in published maps and institutional affiliations.